Supplement of Atmos. Chem. Phys., 22, 12607–12627, 2022
https://doi.org/10.5194/acp-22-12607-2022-supplement

Atmospheric Chemistry and Physics
Open Access
EGU

Supplement of

Ice-nucleating particles near two major dust source regions

Charlotte M. Beall et al.

Correspondence to: Charlotte M. Beall (cbeall@ucsd.edu)

S1 Aerosol density, shape and refractive index values

S1.1 Coarse mode (d_p > 3000 nm)

Table S1.1 Coarse mode particle density, shape, and refractive index values used to convert optical particle diameters to geometric diameters.

Particle type	Density (g ccm^{-1})	Shape	Refractive index
Dust	2.7 (Hinds, 1999; Reitz, 2011)	1.5 (Reitz, 2011)	1.46 – i0.006 (Tegen et al., 1996; Seinfeld and Pandis, 2016)
Sea salt	2.17 (Kulkarni et al., 2011)	1.08 (Hinds, 1999)	1.544 – i0 (Hinds, 1999)

S1.2 Accumulation mode (d_p 700 – 3000 nm)

An average density of 1.529 g cm^{-3} waswas calculated from the measured composition (AMS species + black carbon) according to the method by (Salcedo et al., 2006). Density values for sulfates and nitrates were also taken from this publication. For NH_4Cl, instead of 1.52 g cm^{-3} (Salcedo et al., 2006) the more recent value of 1.53 g cm^{-3} was used (Levin et al., 2010). For organics (1.2 g cm^{-3}) was taken from Levin et al. (2010). For black carbon (1.8 g cm^{-3}), the density was taken from Bond and Bergstrom (2006). The shape of the accumulation mode particles was assumed to be spherical (shape factor = 1).

S2 PM_{10} sampling for sea salt:dust mass-ratio assumption

PM_{10} samples were collected daily on Teflon filters (Zefluor®, Pall Life Sciences, USA) using a low-volume aerosol sampler (ca. 10 L min^{-1}) operated with a Harvard head impactor designed to collect PM_{10}. Filters were stored in a sterile petri dish at -20 °C until gravimetric and chemical analysis. The average fraction of dust and sea salt for the entire duration of the campaign was calculated from the daily PM_{10} samples, weighed for the respective sampling times. The error between the average mass ratio and the mass ratio measured in each daily sample was calculated and included in the error of the particulate surface (PS) values (see S3.3).

S3 Estimation of aerosol surface area concentration uncertainty

As described in Sect. 2.2, the particle surface area concentrations were calculated from FMPS (dp = 5.6 nm – 560 nm) and OPC (dp = 250 nm – 32 µm) measurements. The final particle surface area concentrations have an uncertainty that is the result of several contributions: inlet and transport losses, re-binning uncertainty, FMPS scaling uncertainty and uncertainty due to counting statistics. The details on uncertainty estimation for each component are provided below.

S3.1 Inlet and transport losses

Inlet and transport losses were calculated using the Particle Loss Calculator (von der Weiden et al., 2009). FMPS losses were below 10% for particles larger than 15 nm and below 2% for particles larger than 30 nm. For the OPC the losses were well below 1% up to particles of 3 µm diameter and reach 10% for particles of 6 µm diameter.

Since most (~75%) of the particle surface area concentration is found between 30 nm and 1 µm (where losses are between 2% and 0.2%) and most of the rest is found between 1 µm and 7 µm (where losses increase from 0.2% to 20%), overall losses of the particle surface concentration are less than 3%.

S3.2 Instrumental measurement uncertainty of FMPS and OPC

Measurement uncertainty of the FMPS and OPC, e.g.,. as a consequence of calibration uncertainties or uncertainties of the flow rates, have been determined by co-located measurements with other instruments over extended time intervals. The OPC and FMPS uncertainty per size bin are 10 and 15%, respectively.

S3.3 Re-binning uncertainty

For calculation of the surface area concentrations, geometric diameters have been calculated from optical particle diameters for the OPC measurements. This re-binning requires making assumptions about the composition of the coarse particles (fraction of dust and sea salt, respectively) and about the optical properties of the fine particles (chemical composition taken from AMS and BC measurements; see Sects. S1-2). The ensuing uncertainty in the calculated particle diameter of the re-binned size distribution results in uncertainties of the calculated surface concentration. From sensitivity tests we estimate the resulting uncertainties from re-binning for the particle surface concentration to be around 5%.

S3.4 FMPS scaling uncertainty

A scaling factor of 1.3 (with an uncertainty of 10%) was applied to PS_1 to correct for under-measurement of particles in the upper measurement range of the FMPS (above ca. 100 nm). As a consequence of low-biased particle concentration measurements in the FMPS, the calculated surface concentrations were too low. To correct for this effect, the FMPS and OPC data were merged again, not averaging the overlap size bins but interpolating from the upper end of the correct FMPS data up to the lower end of the OPC. From comparison of the result of this exercise with the previous calculations, a correction factor for particulate surface area < 1 µm (PS_1) of 1.3 (with an uncertainty of 10%) was determined. The particulate surface area < 10 µm (PS_{10}) concentrations were corrected accordingly by accounting for the corrected PS_1 contribution. From temporal variability of this scaling factor, we estimate the uncertainty of this effect to result in an uncertainty of the particle surface concentration of 10%.

S3.5 Uncertainty due to counting statistics

Relative uncertainties due to counting statistics were calculated from the average number of particles per size bin as measured during a sampling interval of 60 s (probed volume = 1200 cm^3) for different size bins. Smaller sizes have smaller relative uncertainties due to larger numbers of counted particles (see examples in Table below).

Particle diameter (μm)	Average number concentration (cm^{-3})	Average sampling rate (min^{-1})	Relative uncertainty (%)
1	1	1200	3
5	0.04	50	14
10	0.004	5	45

From the average surface distribution, we find that particles smaller than 1 μm in diameter with a counting statistics uncertainty below 3% contribute ~75% of the surface area; 25% of the surface area is found for particles between about 1 μm and 8 μm with an estimated average counting statistics uncertainty of about 15%. Therefore, we estimate that the overall counting statistics-related uncertainty of the particle surface concentration is in the order of 5-7% for 1-minute averages.

Considering all the components to the overall particle surface concentration uncertainty described above, we conservatively estimate the uncertainty of the particle surface concentration to be 30%. The only systematic bias is due to the inlet losses, which were estimated to have an effect of less than 3% on the total surface concentration.

S4 Description of MERRA-2 Dust Simulations

MERRA-2 simulates 5 types of aerosols (dust, sea salt, sulfate, and black and organic carbon) using the Goddard Chemistry, Aerosol, Radiation, and Transport (GOCART) model (Chin et al., 2002; Colarco et al., 2010). Dust emissions and deposition rates in MERRA-2 are estimated by summing the emissions and deposition rates across GOCART simulated dust particles between 0.1 - 10 μm in size (dry diameter) (Gelaro et al., 2017). Dust emissions are constrained by wind-driven erosion over the source locations, which are identified from the topographic depression map (Ginoux et al., 2001). Aerosol observations are derived from various satellite products and are jointly assimilated within GEOS-5 with meteorological observations (Buchard et al., 2017). MERRA-2 has been shown to successfully reproduce the interannual variability of North-Atlantic dust transport. Additionally, the improved aerosol assimilation scheme in MERRA-2 was shown to have a positive impact on the representation of long-range dust transport from the Sahara compared to prior versions (Buchard et al., 2017).

S5 FLEXPART Back Trajectories

Air mass 72-hour back-trajectories for each sample were simulated using the FLEXible PARTicle dispersion model (FLEXPART) in backward mode (Stohl et al., 1998). NOAA Climate Forecast System (CFS) short-duration ($t < 6$ h) forecasts (Saha et al., 2014) were used as three-dimensional forcing datasets. Particle releases ($n = 2000$) from 35 m above sea level (ASL) followed the vessel track using vessel position information from the European Common Automatic Weather Station (EUCAWS; http://eumetnet.eu/; last access Sept. 2021) for the duration of each sampling period.

S6 HYSPLIT/STILT Source Footprints

Source footprints (Figs. S11-S16) were calculated using the Hybrid Single-Particle Lagrangian Integrated Trajectory model (HYSPLIT) with the Stochastic Time-Inverted Lagrangian Transport (STILT) dispersion module, which is optimized for backward-in-time dispersion simulations to determine source

regions of receptors (Loughner et al., 2021; Stein et al., 2015). The computation is based on emitting a large number of computational “particles” at the receptor location, which are tracked backwards in time subject to stochastic variations in turbulent processes. The influence of a given surface element within the area covered by the particle trajectories is then proportional to the number of particles that have been present close to the surface within the time over which the integration is performed. Here, we emitted 10,000 particles during each hour that sampling was conducted at the ship’s location at 10 m a.g.l. The particles were then tracked backwards for 72 h, a typical residence time of a coarse particle in the atmosphere, and their concentration in the lower 500 m a.g.l. was averaged over this time. The meteorological data from the Global Forecast System (GFS) at a resolution of 0.25º were used in the calculations. Tests using 1º data from the NCEP Global Data Assimilation System (GDAS) model yielded similar results. For consistent visualization, the particle concentrations were normalized to a value of 100% at the location of maximum concentration, which is very close to the ship’s location.

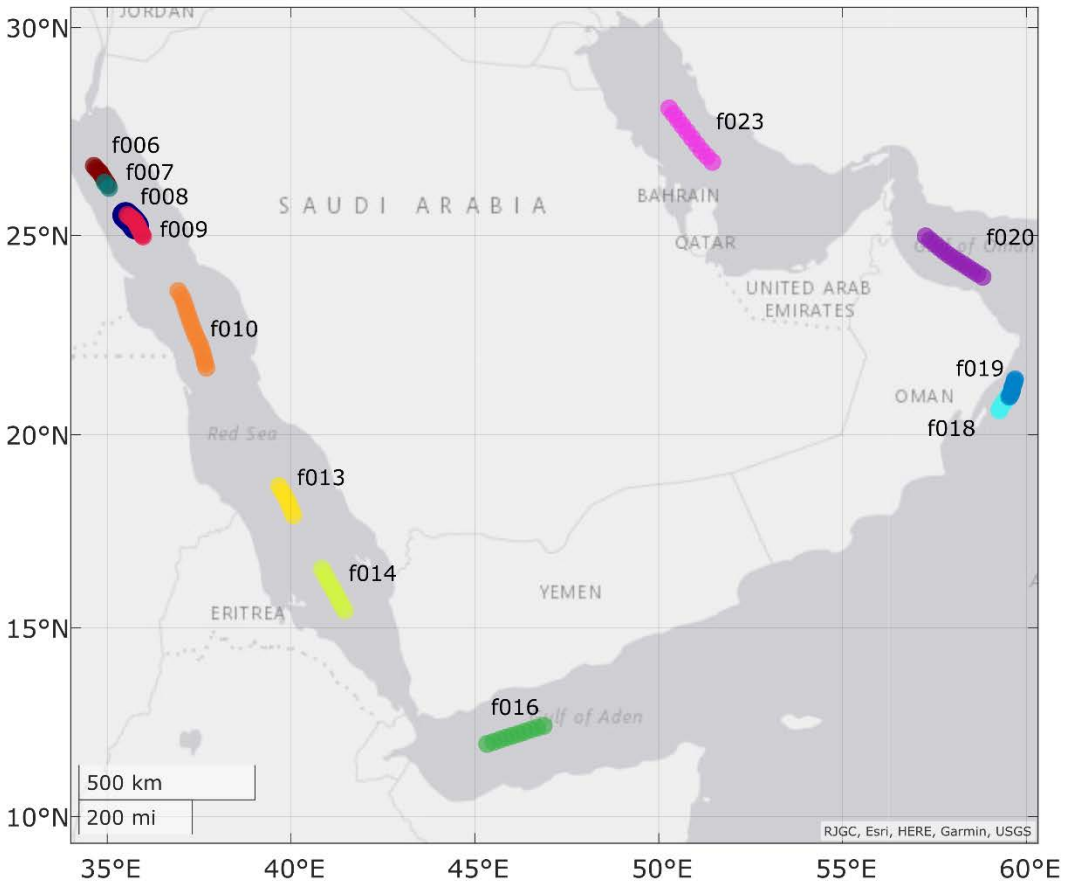

Figure S1. Locations where each aerosol sample was collected during Leg 1 (Malta to Kuwait).

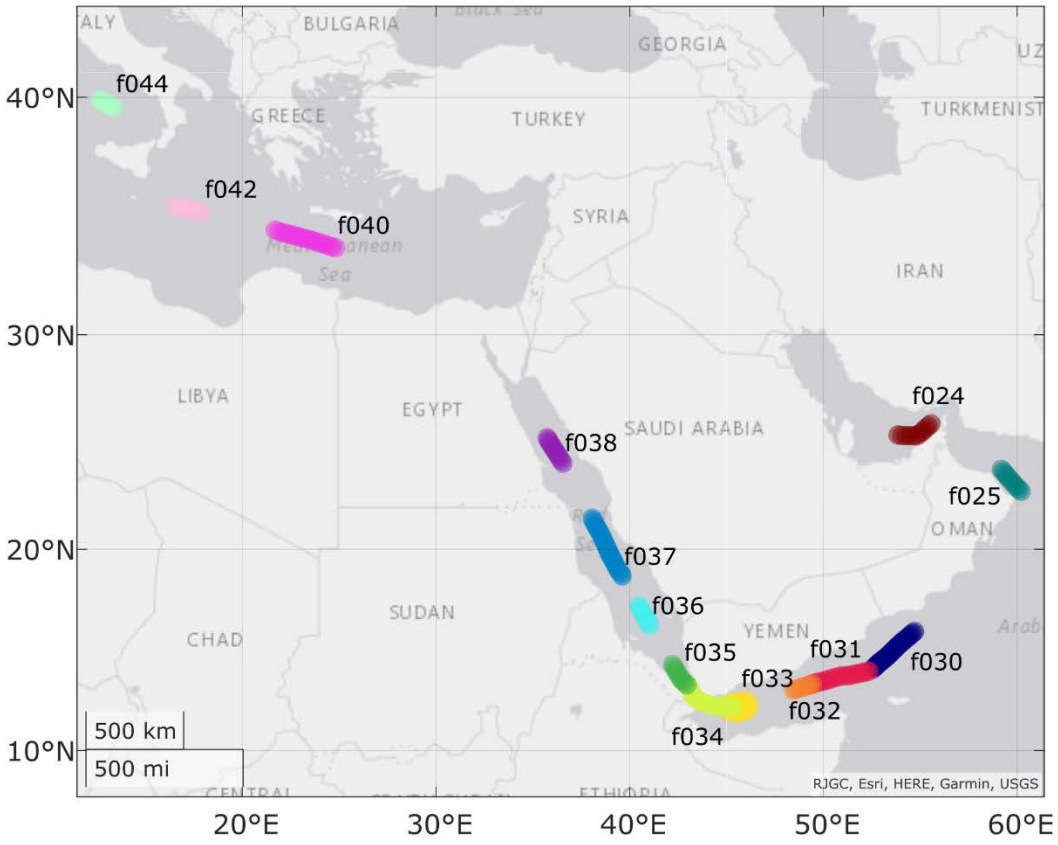

Figure S2. Locations where each aerosol sample was collected during Leg 2 (Kuwait to Toulon).

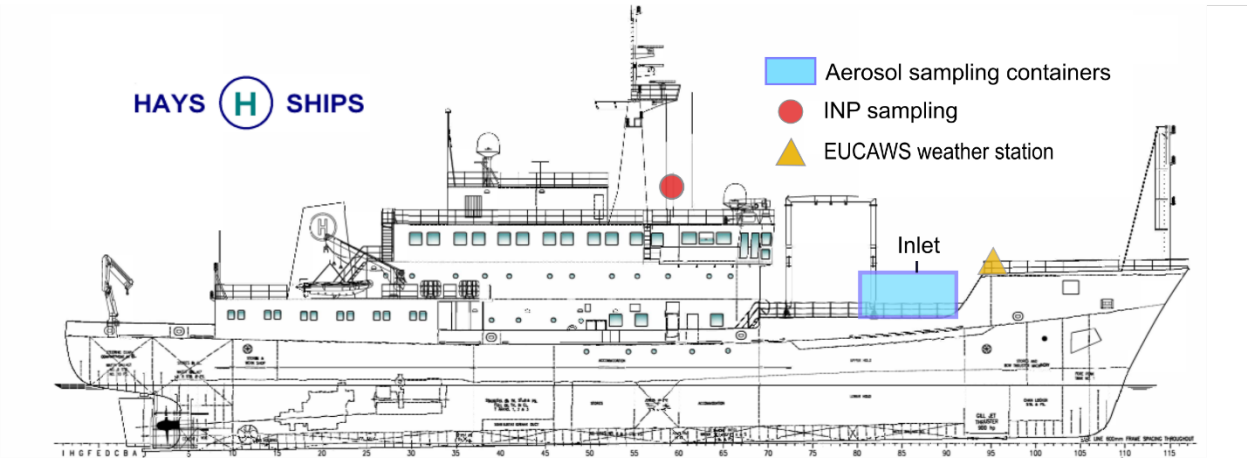

Figure S3. Aerosol sampling, INP sampling and weather station locations on the RV *Kommandor Iona*.

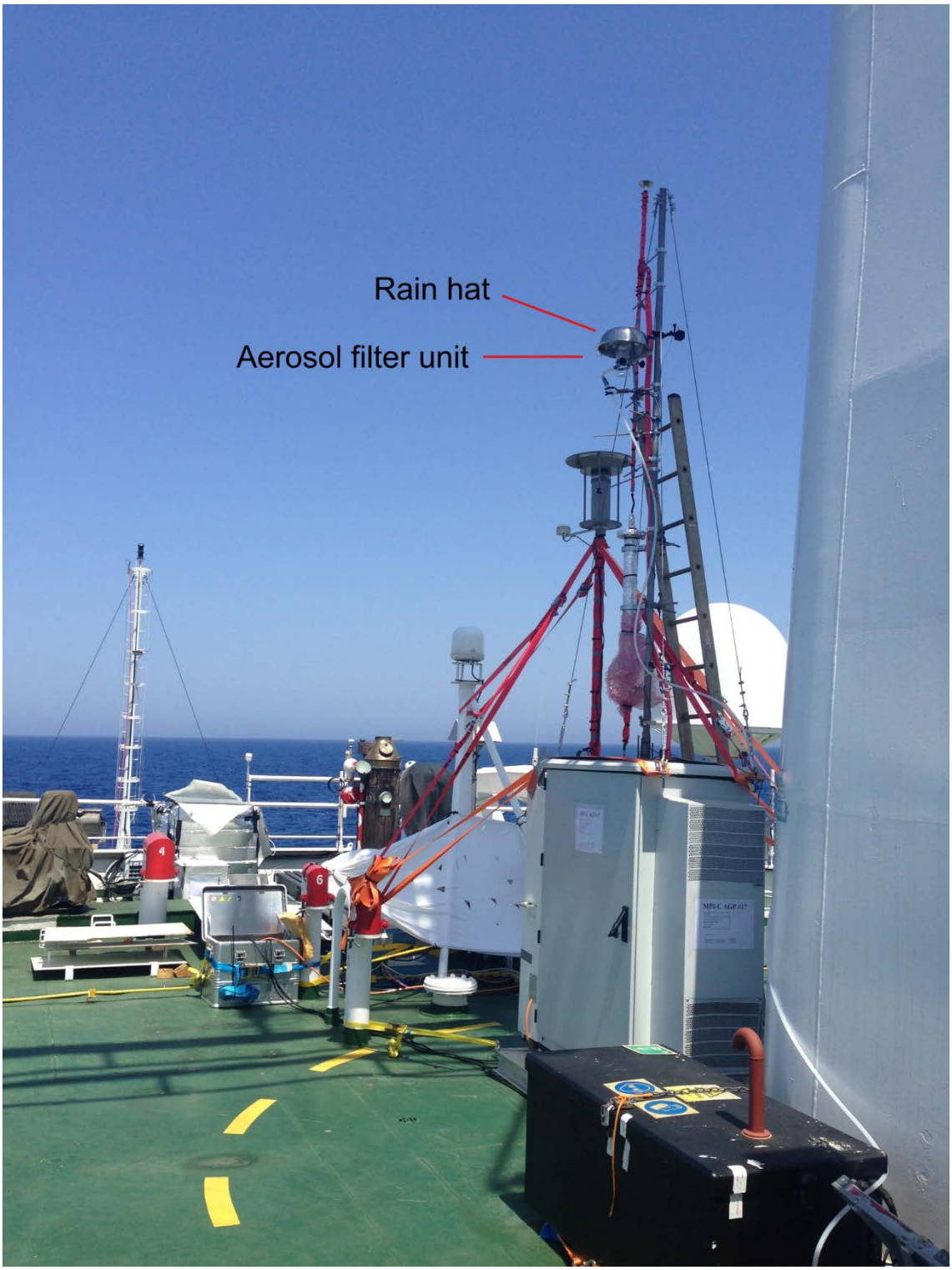

Figure S4. INP sampling set-up on the RV *Kommandor Iona* wheelhouse top.

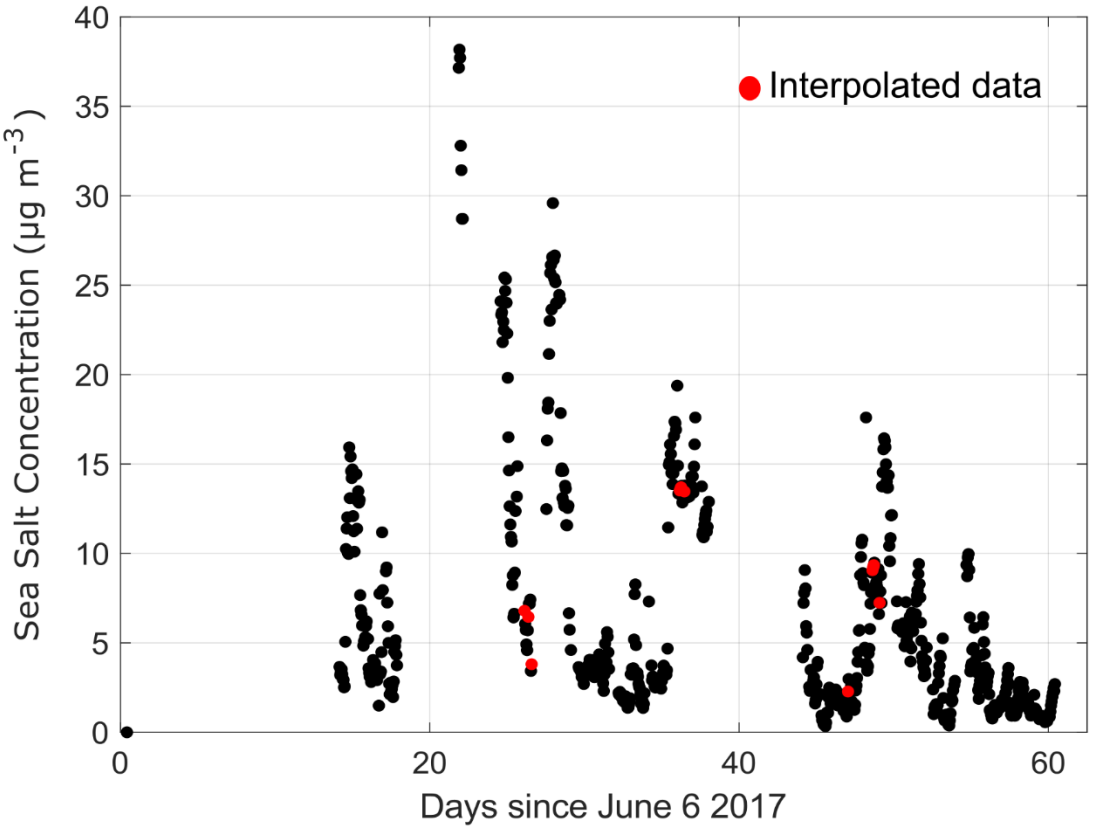

Figure S5. Time series of sea salt concentrations in aerosol. Sea salt concentrations were estimated from soluble Na^+ concentrations measured in total suspended particles (Sect. 2.2) and were used as a proxy for SSA number concentrations. Red markers show where hourly composition data was linearly interpolated for four samples where data was partially missing (samples f020, f025, f036 and f037).

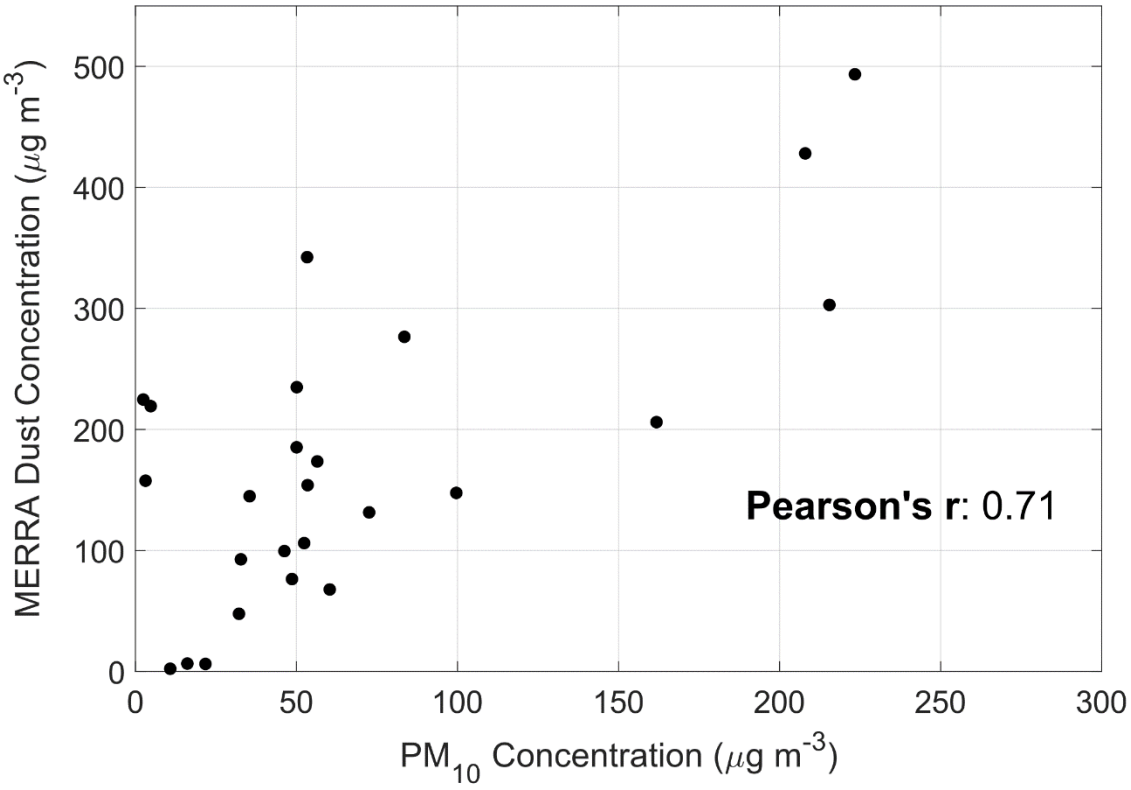

Figure S6. Comparison of MERRA-2 surface dust mass concentrations and observed PM_{10} during INP sampling periods.

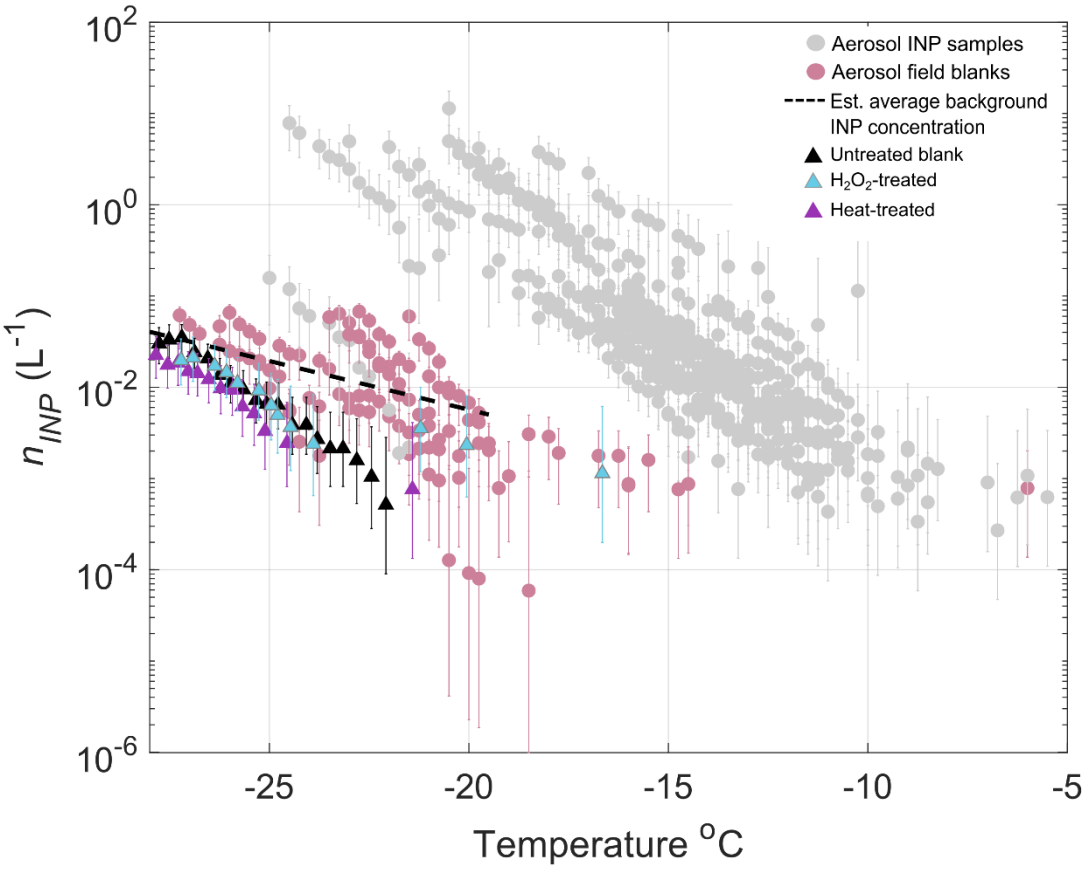

Figure S7. INP concentrations (n_{INP}) measured in 26 aerosol samples collected during AQABA, simulated INP concentrations from 7 blank filter samples, and simulated n_{INP} in a heat-treated and H_2O_2-treated blank filter sample. The simulated blank filter n_{INP} were estimated for the mean volume sampled during AQABA (6680 L, see Methods Sect. 2.4). The freezing onset temperatures detected in 6 of the 7 field blanks ranged between -15 and -27 °C, with the exception of one field blank sample in which a single freezing event was detected at a relatively higher temperature of -6 °C. This indicates the presence of a rare contaminant with a high freezing temperature from sampling handling processes, as this single freezing event represented 1/255 of total detected field blank freezing events. The n_{INP} measured in one aerosol sample (f033) fell within the range of background INP levels present in field blanks.

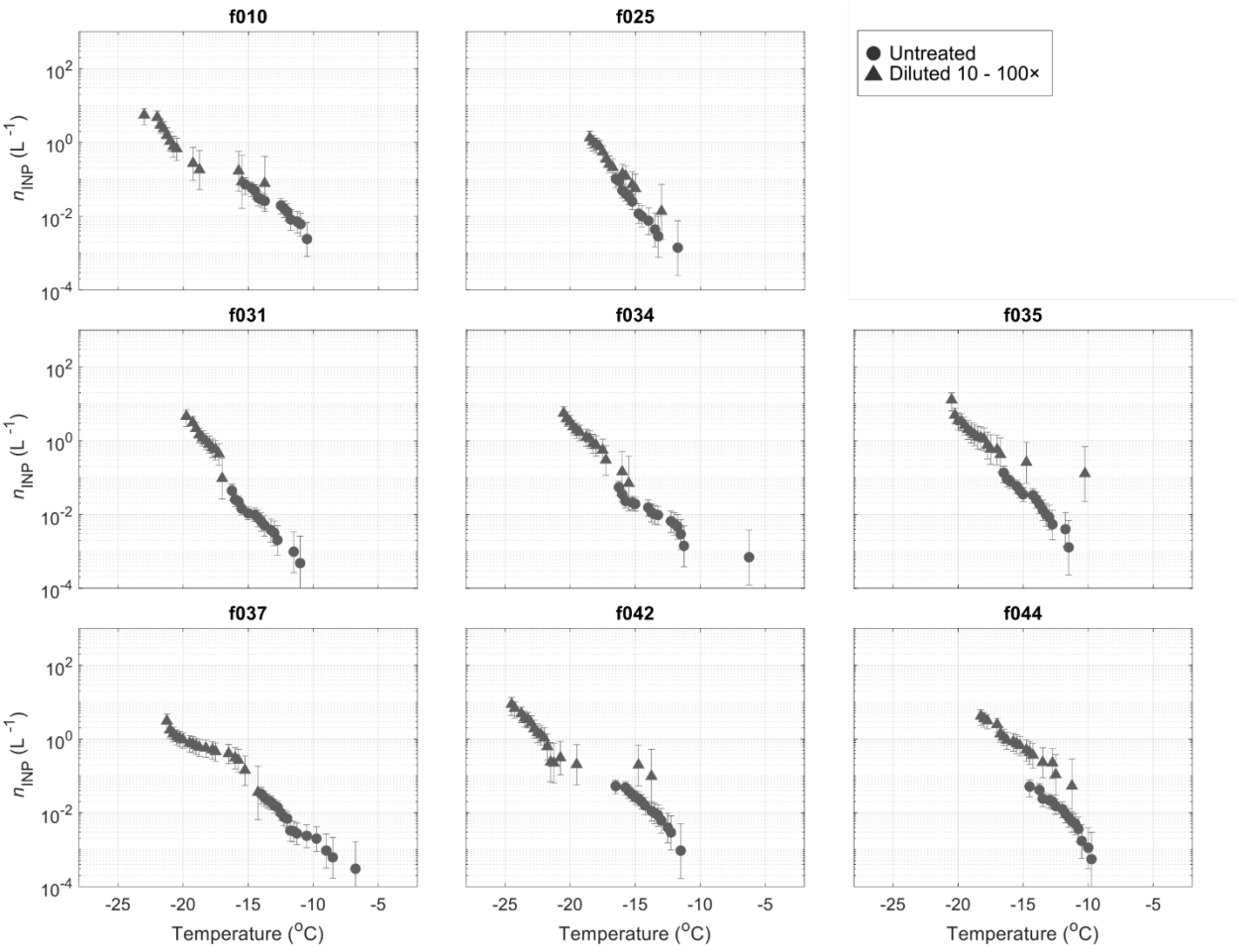

Figure S8. INP concentrations (n_{INP}) measured in 8 aerosol samples from which a dilution was performed (10-100×). The n_{INP} spectra from both the original suspension and the dilution are shown (see Methods Sect. 2.4).

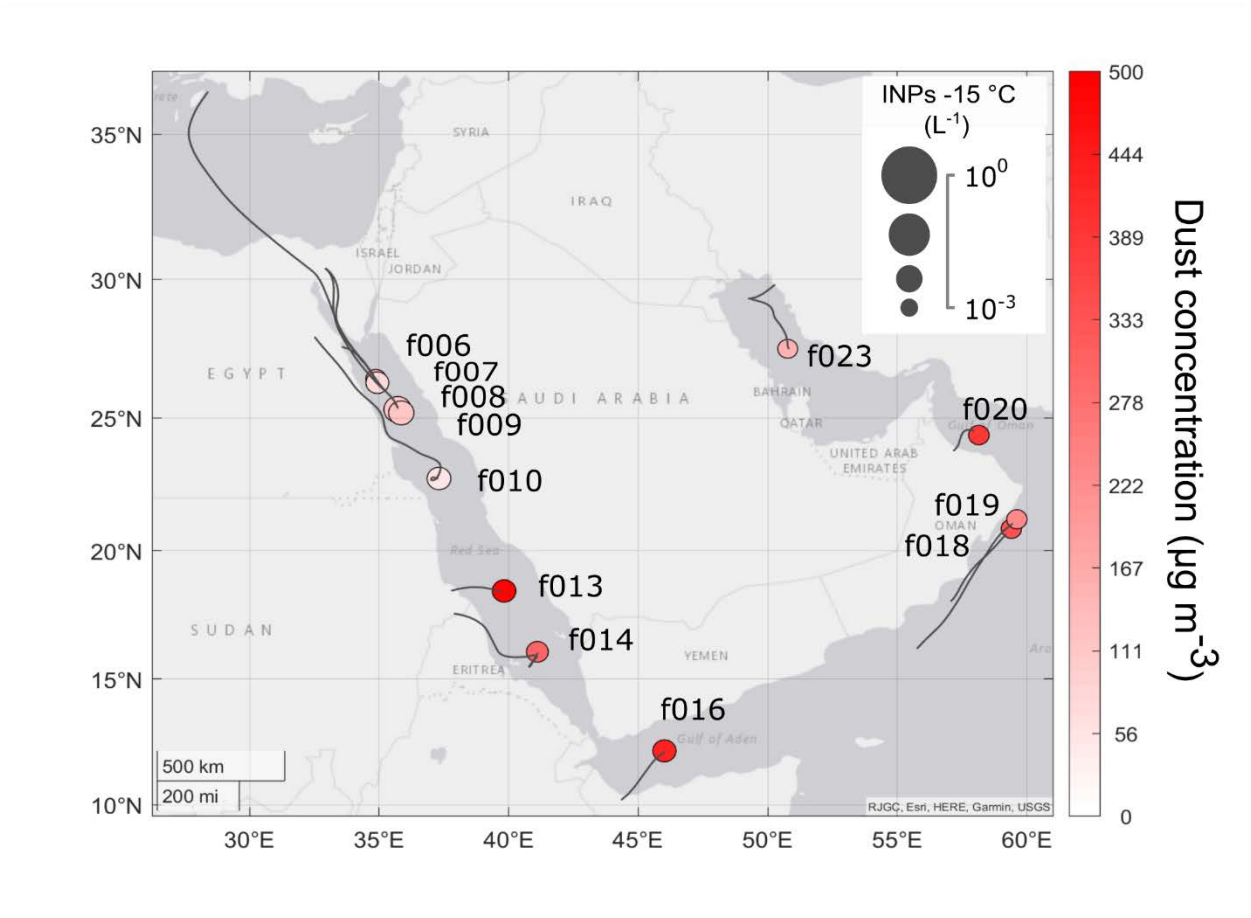

Figure S9. Aerosol 72-hour back trajectories for Leg 1 simulated by FLEXPART (Sect. S5).

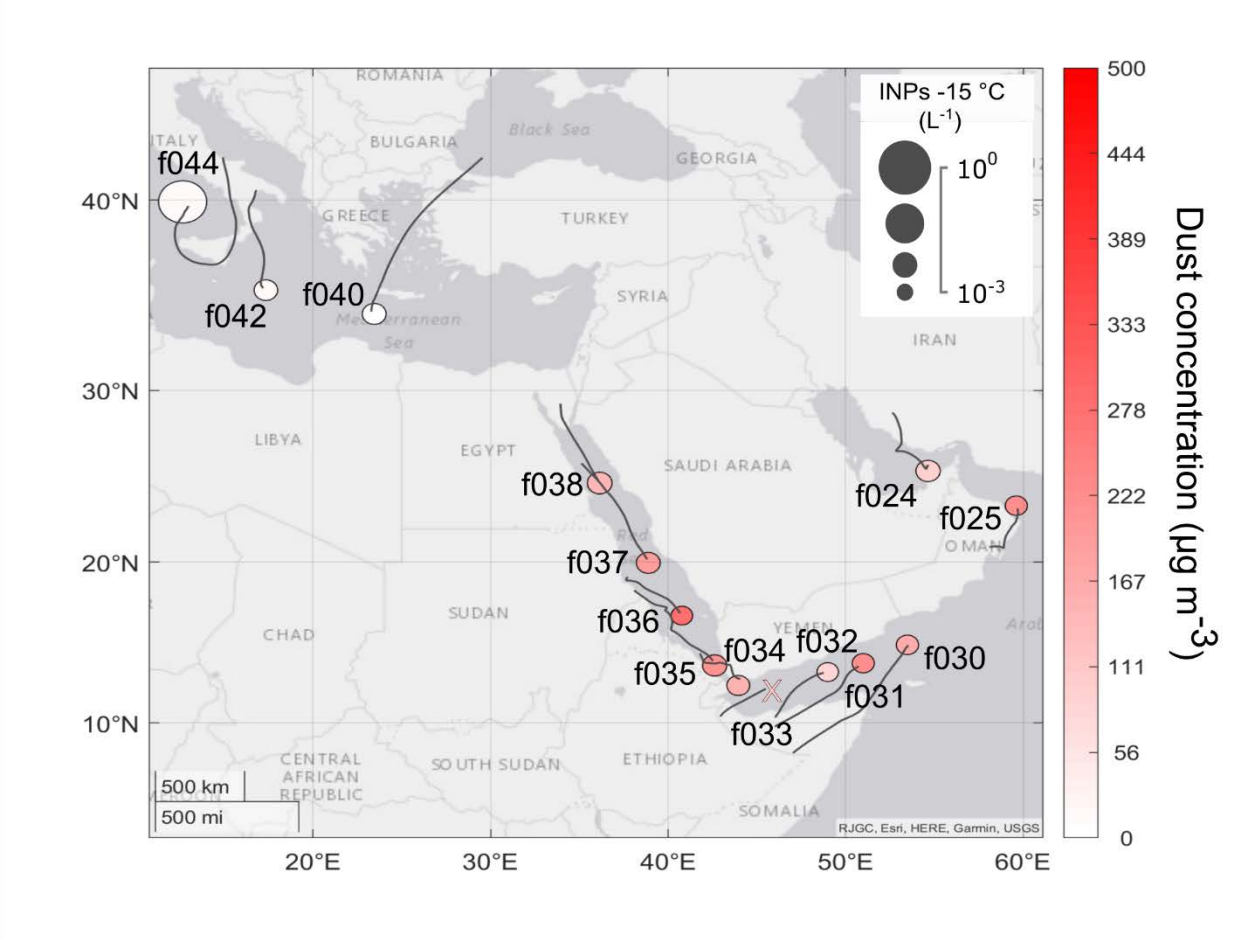

Figure S10. Aerosol 72-hour back trajectories for Leg 2 simulated by FLEXPART (Sect. S5). Sample f033 marked with an X to indicate no INPs detected at -15 °C.

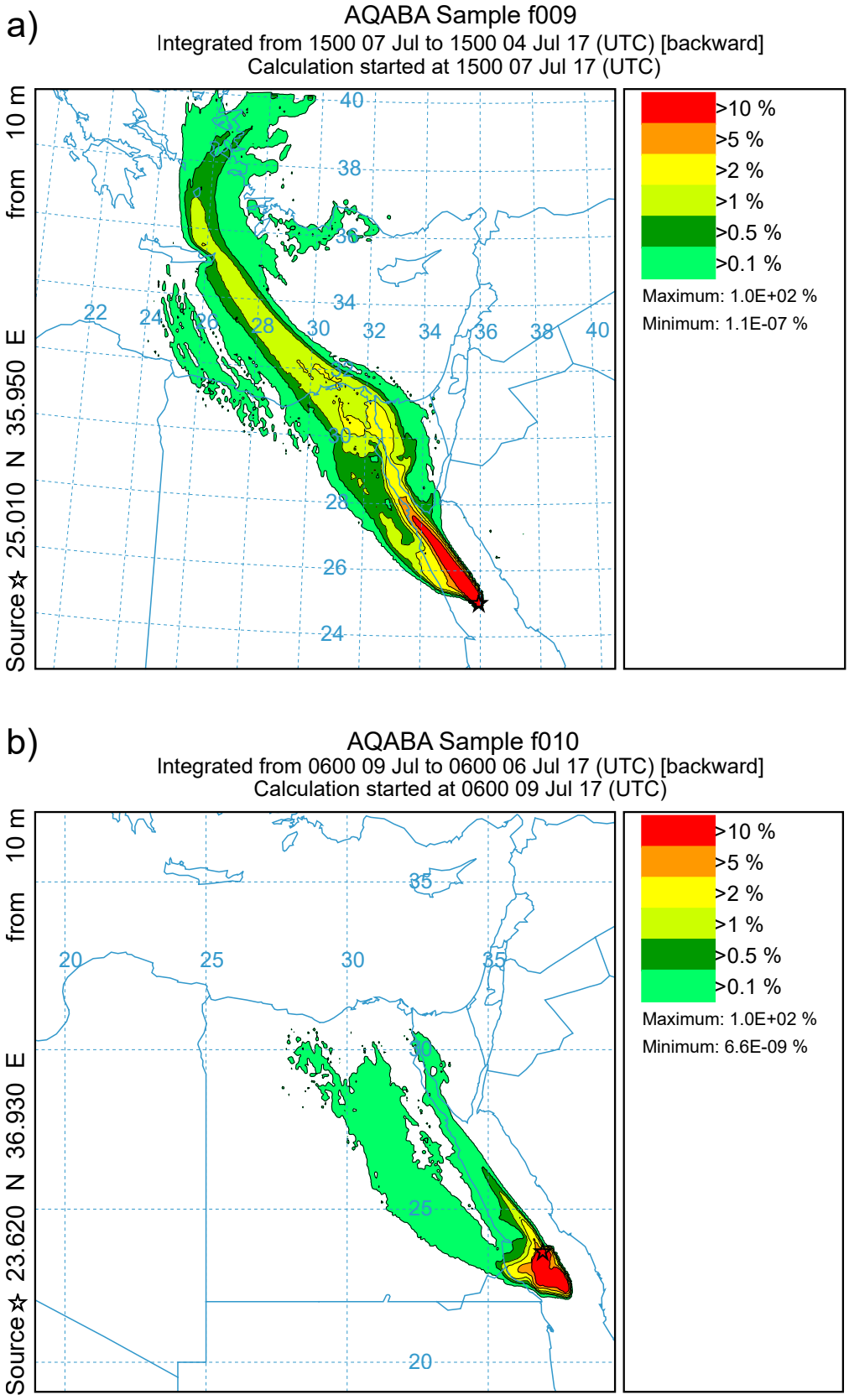

Figure S11. Footprint plots for samples (a) f009 and (b) f010. The footprints were calculated using the HYSPLIT dispersion model running in backward mode with the STILT algorithm. The runs were intitiated at the midpoint location of the sample collection ("SOURCE") at 10 m a.g.l. and computational "particles" were emitted over the time of sample collection. The plot shows "particle" concentrations from the ground to 500 m a.g.l. averaged over 72 h and normalized to the maximum particle concentration.

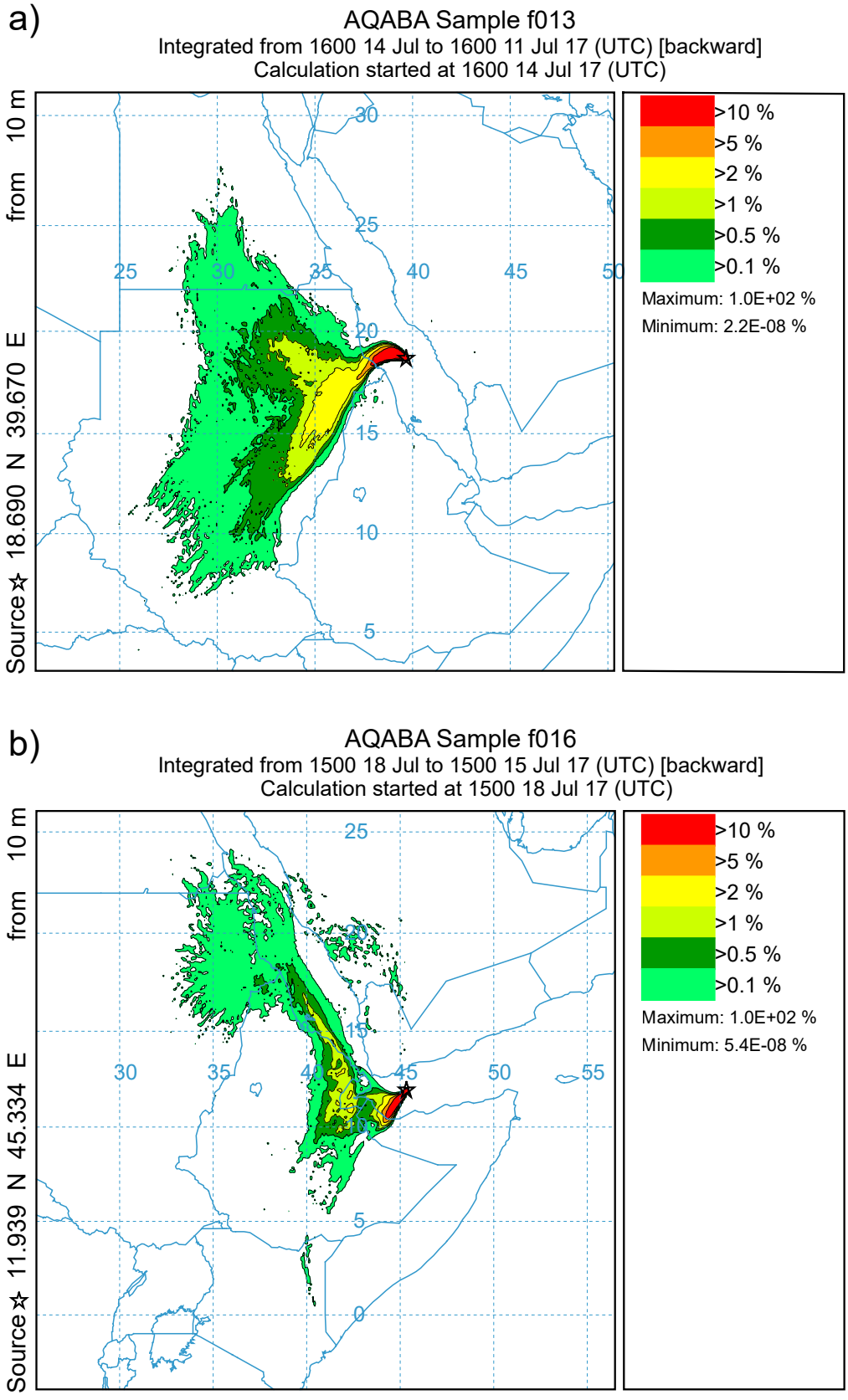

Figure S12. Footprint plots for samples (a) f013 and (b) f016. The footprints were calculated using the HYSPLIT dispersion model running in backward mode with the STILT algorithm. The runs were intitiated at the midpoint location of the sample collection ("SOURCE") at 10 m a.g.l. and computational "particles" were emitted over the time of sample collection. The plot shows "particle" concentrations from the ground to 500 m a.g.l. averaged over 72 h and normalized to the maximum particle concentration.

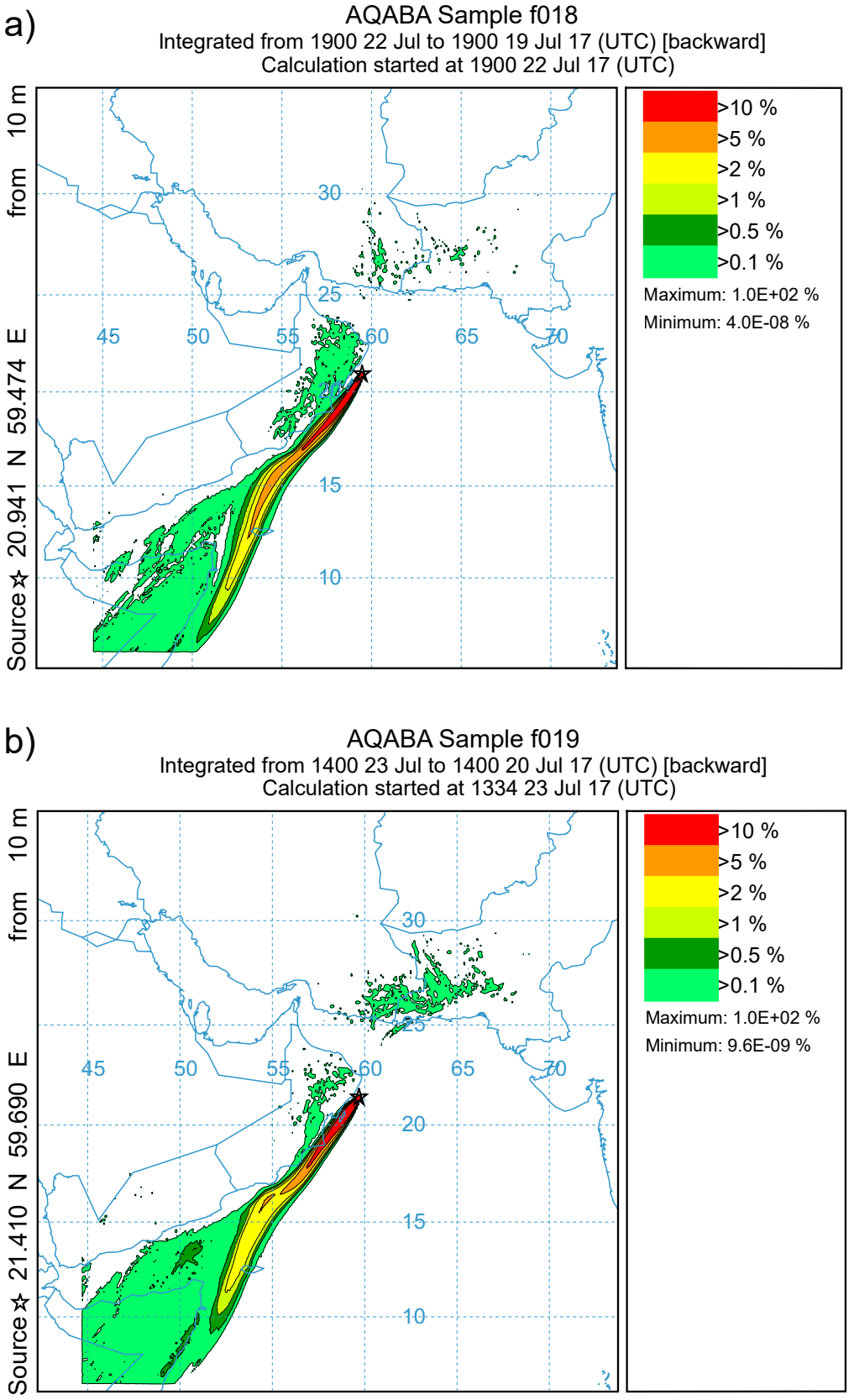

Figure S13.: Footprint plots for samples (a) f018 and (b) f019. The footprints were calculated using the HYSPLIT dispersion model running in backward mode with the STILT algorithm. The runs were intitiated at the midpoint location of the sample collection ("SOURCE") at 10 m a.g.l. and computational "particles" were emitted over the time of sample collection. The plot shows "particle" concentrations from the ground to 500 m a.g.l. averaged over 72 h and normalized to the maximum particle concentration.

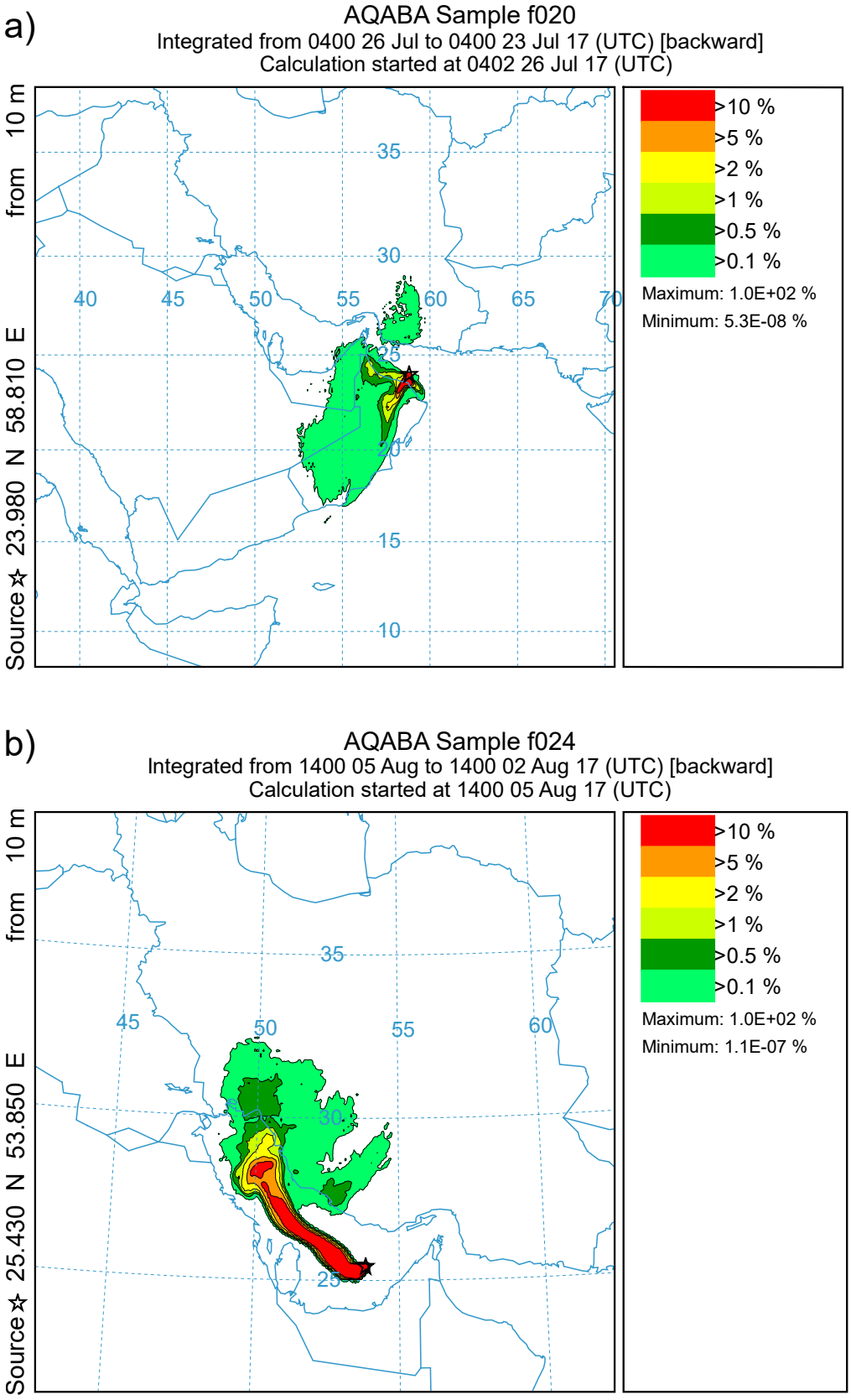

Figure S14. Footprint plots for samples (a) f020 and (b) f024. The footprints were calculated using the HYSPLIT dispersion model running in backward mode with the STILT algorithm. The runs were intitiated at the midpoint location of the sample collection ("SOURCE") at 10 m a.g.l. and computational "particles" were emitted over the time of sample collection. The plot shows "particle" concentrations from the ground to 500 m a.g.l. averaged over 72 h and normalized to the maximum particle concentration.

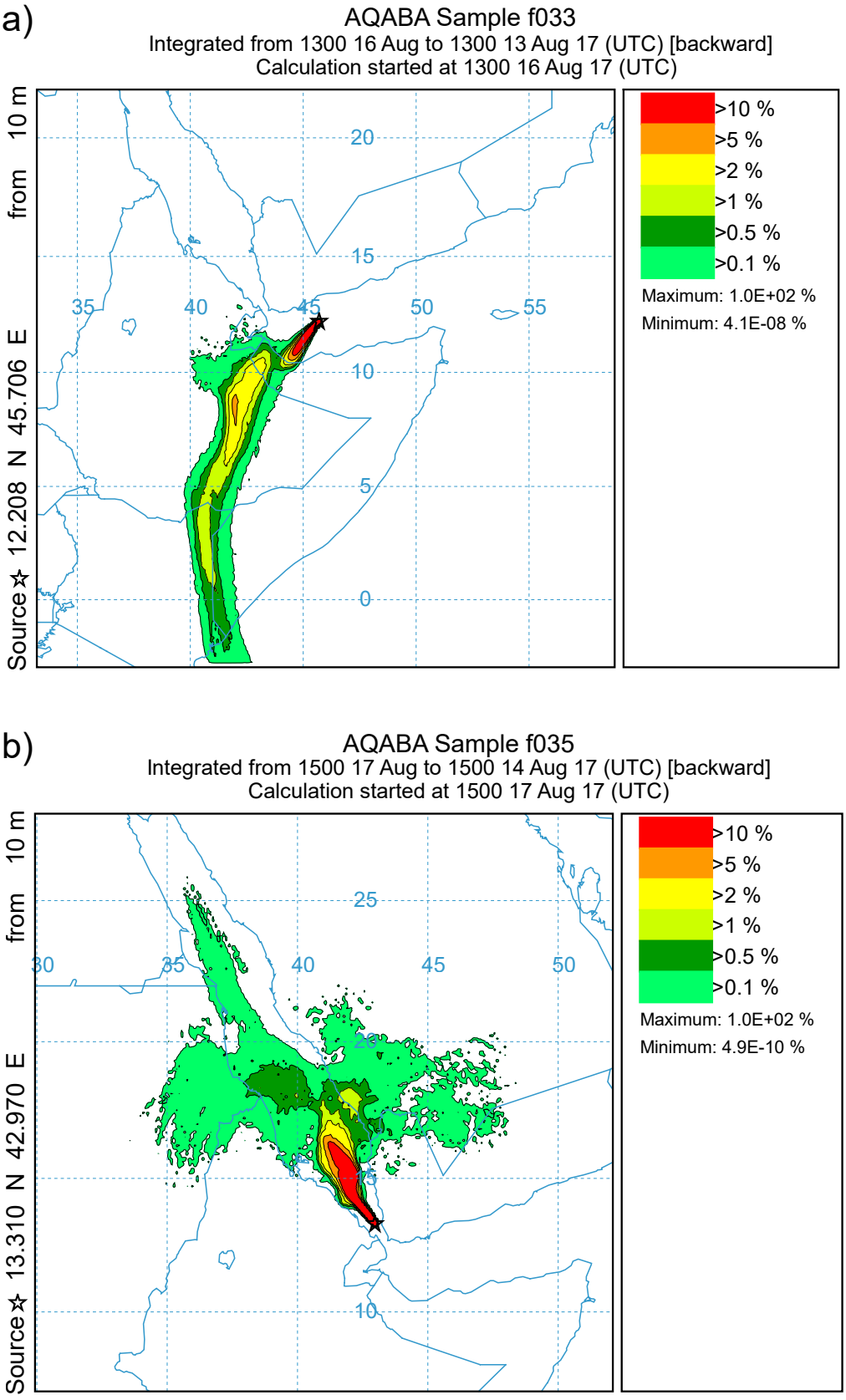

Figure S15. Footprint plots for samples (a) f033 and (b) f035. The footprints were calculated using the HYSPLIT dispersion model running in backward mode with the STILT algorithm. The runs were intitiated at the midpoint location of the sample collection ("SOURCE") at 10 m a.g.l. and computational "particles" were emitted over the time of sample collection. The plot shows "particle" concentrations from the ground to 500 m a.g.l. averaged over 72 h and normalized to the maximum particle concentration.

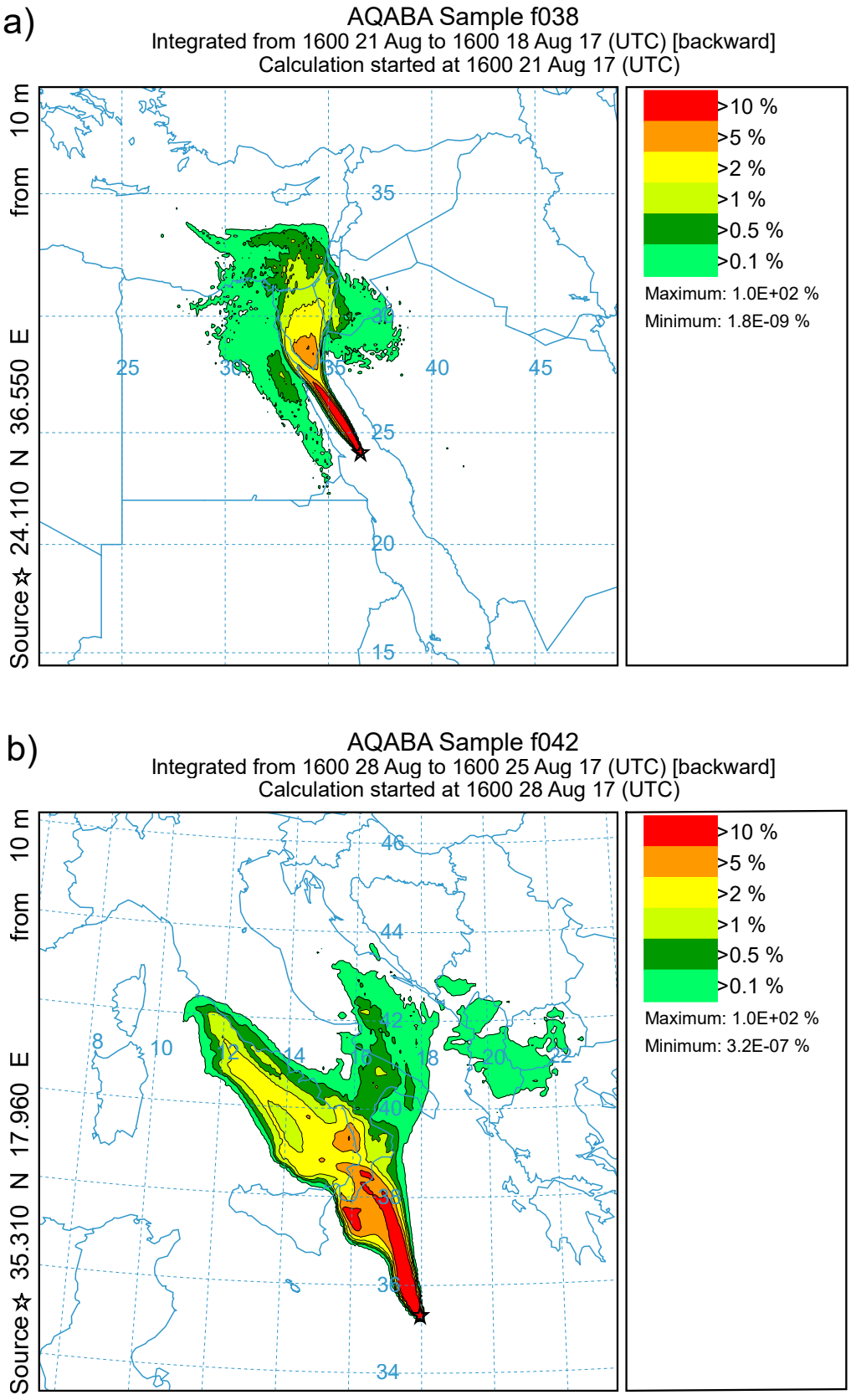

Figure S16. Footprint plots for samples (a) f038 and (b) f042. The footprints were calculated using the HYSPLIT dispersion model running in backward mode with the STILT algorithm. The runs were intitiated at the midpoint location of the sample collection ("SOURCE") at 10 m a.g.l. and computational "particles" were emitted over the time of sample collection. The plot shows "particle" concentrations from the ground to 500 m a.g.l. averaged over 72 h and normalized to the maximum particle concentration.

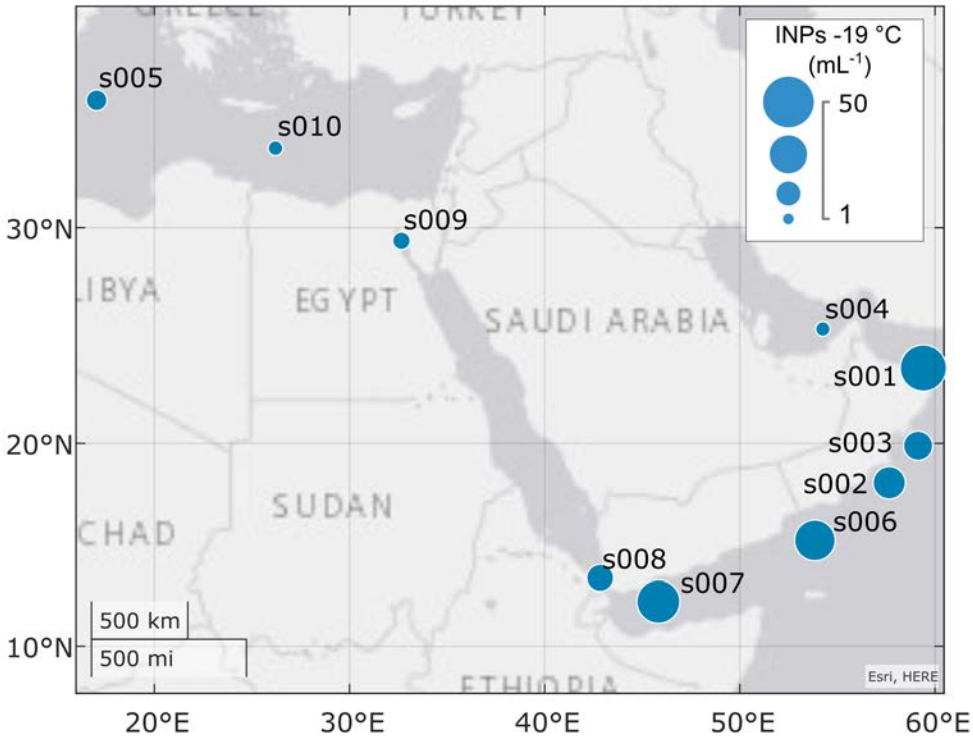

Figure S17. Map of the collection locations of 10 subsurface seawater (SSW) samples. Marker sizes indicate abundance of INPs.

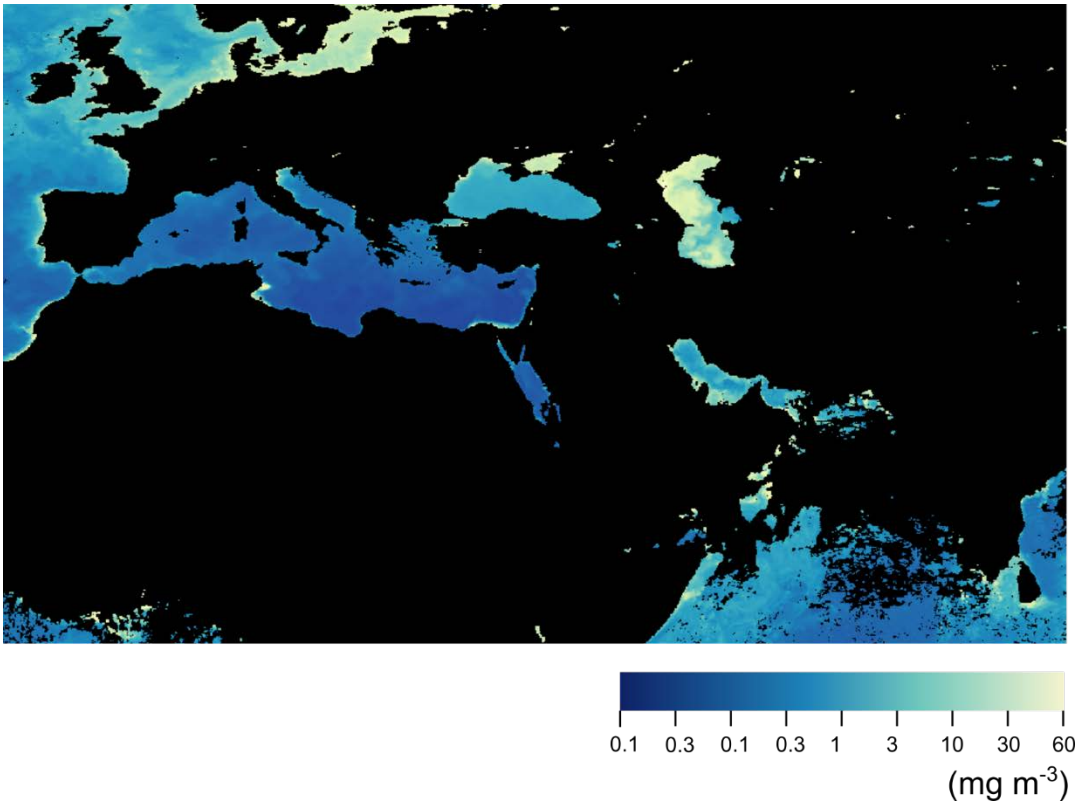

Figure S18. Average ocean surface chlorophyll *a* concentration from 1 August to 31 August 2017 (Moderate Resolution Imaging Spectroradiometer, https://oceandata.sci.gsfc.nasa.gov/MODIS-Aqua).

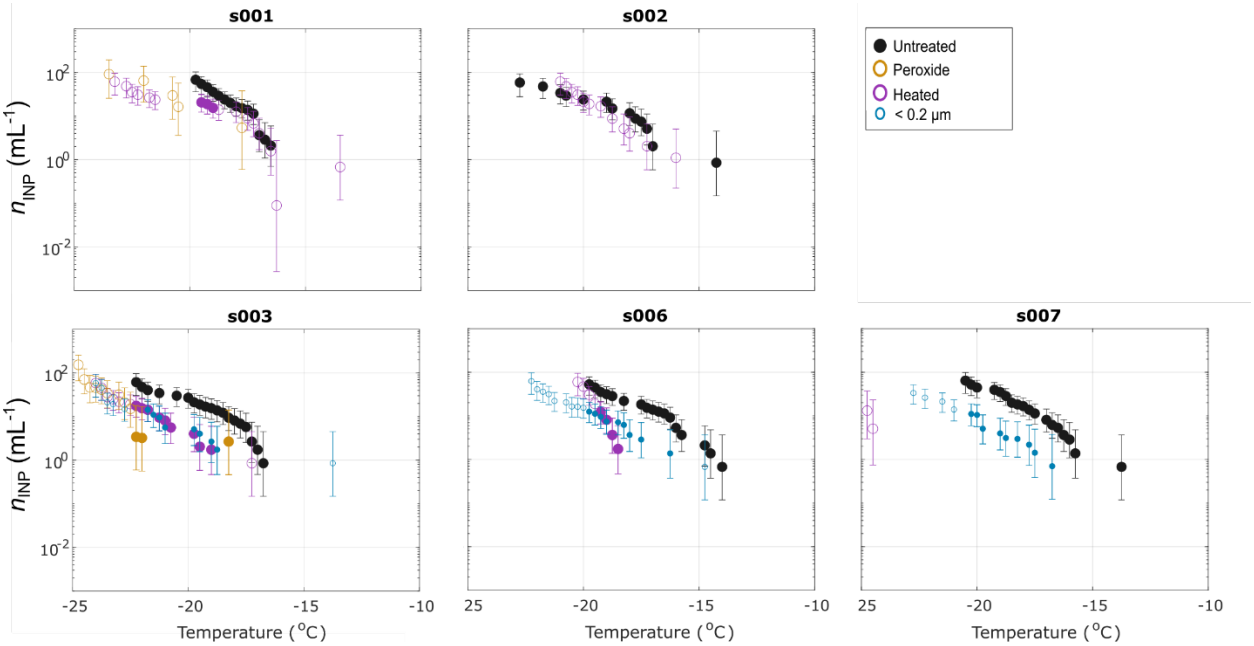

Figure S19. Measured concentrations of INPs in SSW samples that were treated with heat, hydrogen peroxide and a 0.2 µm filter (Methods Sec. 2.5). Markers of heat-treated, filtered, and H_2O_2-treated samples are filled to indicate significant n_{INP} difference from untreated samples according to Fisher's Exact Test ($p < 0.05$). Results indicate the presence of organic, heat-labile and heat-stable INPs, and an abundance of INPs both larger and smaller than 0.2 µm.

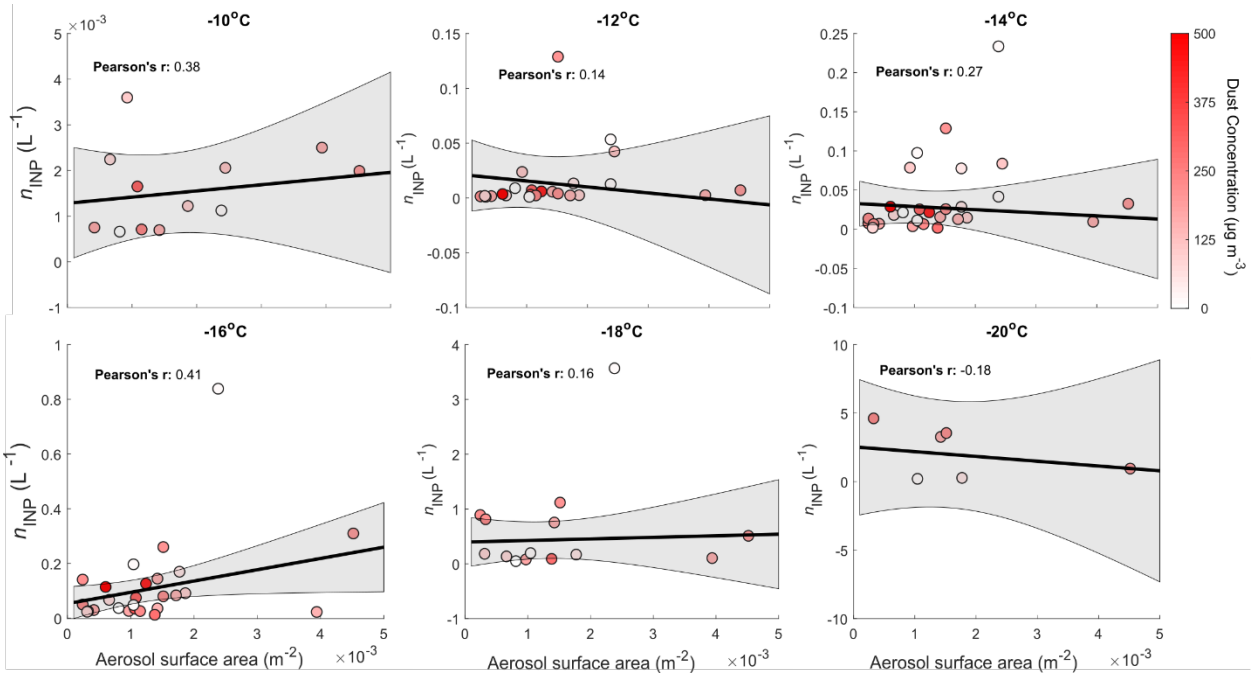

Figure S20. Linear regressions between total aerosol surface area and concentrations of INPs with freezing temperatures between -10 and -20 °C. Results show little to no correlation between n_{INP} and total aerosol surface area. Shaded region is the 95% confidence interval for the best fit linear regression. Marker colors indicate the average ambient dust mass concentration during the sampling period. Dilutions of 8 filter samples are included in the regression analysis (Fig. S8).

References

Bond, Tami C. and Bergstrom, Robert W.: Light absorption by carbonaceous particles: An investigative review, https://doi.org/10.1080/02786820500421521, 2006.

Buchard, V, Randles, C A, da Silva, A M, Darmenov, A, Colarco, P R, Govindaraju, R, Ferrare, R, Hair, J, Beyersdorf, A J, Ziemba, L D, and Yu, H: The MERRA-2 Aerosol Reanalysis, 1980 Onward. Part II: Evaluation and Case Studies, J. Clim., 30, 6851–6872, https://doi.org/10.1175/JCLI-D-16-0613.1, 2017.

Chin, Mian, Ginoux, Paul, Kinne, Stefan, Torres, Omar, Holben, Brent N, Duncan, Bryan N, Martin, Randall V, Logan, Jennifer A, Higurashi, Akiko, and Nakajima, Teruyuki: Tropospheric Aerosol Optical Thickness from the GOCART Model and Comparisons with Satellite and Sun Photometer Measurements, J. Atmos. Sci., 59, 461–483, https://doi.org/10.1175/1520-0469(2002)059<0461:TAOTFT>2.0.CO;2, 2002.

Colarco, Peter, da Silva, Arlindo, Chin, Mian, and Diehl, Thomas: Online simulations of global aerosol distributions in the NASA GEOS-4 model and comparisons to satellite and ground-based aerosol optical depth, J. Geophys. Res. Atmos., 115, https://doi.org/https://doi.org/10.1029/2009JD012820, 2010.

Gelaro, Ronald, McCarty, Will, Suárez, Max J, Todling, Ricardo, Molod, Andrea, Takacs, Lawrence, Randles, Cynthia A, Darmenov, Anton, Bosilovich, Michael G, Reichle, Rolf, Wargan, Krzysztof, Coy, Lawrence, Cullather, Richard, Draper, Clara, Akella, Santha, Buchard, Virginie, Conaty, Austin, da Silva, Arlindo M, Gu, Wei, Kim, Gi-Kong, Koster, Randal, Lucchesi, Robert, Merkova, Dagmar, Nielsen, Jon Eric, Partyka, Gary, Pawson, Steven, Putman, William, Rienecker, Michele, Schubert, Siegfried D, Sienkiewicz, Meta, and Zhao, Bin: The Modern-Era Retrospective Analysis for Research and Applications, Version 2 (MERRA-2), J. Clim., 30, 5419–5454, https://doi.org/10.1175/JCLI-D-16-0758.1, 2017.

Ginoux, Paul, Chin, Mian, Tegen, Ina, Prospero, Joseph M, Holben, Brent, Dubovik, Oleg, and Lin, Shian-Jiann: Sources and distributions of dust aerosols simulated with the GOCART model, J. Geophys. Res. Atmos., 106, 20255–20273, https://doi.org/https://doi.org/10.1029/2000JD000053, 2001.

Hinds, William C: Aerosol Technology Properties, Behavior, and Measurement ofAirborne Particles Second Edition, J. Aerosol Sci., 14, 1999.

Kulkarni, Pramod, Baron, Paul A., and Willeke, Klaus: Aerosol Measurement: Principles, Techniques, and Applications: Third Edition, https://doi.org/10.1002/9781118001684, 2011.

Levin, E. J.T., McMeeking, G. R., Carrico, C. M., Mack, L. E., Kreidenweis, S. M., Wold, C. E., Moosmüller, H., Arnott, W. P., Hao, W. M., Collett, J. L., and Malm, W. C.: Biomass burning smoke aerosol properties measured during Fire Laboratory at Missoula Experiments (FLAME), J. Geophys. Res. Atmos., 115, https://doi.org/10.1029/2009JD013601, 2010.

Loughner, C.P., Fasoli, B., Stein, A.F., Lin, J.C., 2021. Incorporating features from the Stochastic Time-Inverted Lagrangian Transport (STILT) Model into the Hybrid Single-Particle Lagrangian Integrated Trajectory (HYSPLIT) model: A unified dispersion model for time-forward and time-reversed applications, Journal of Applied Meteorology and Climatology 60, 799-810, 10.1175/JAMC-D-20-0158.1.

Reitz, Paul: Chemical composition measurements of cloud condensation nuclei and ice nuclei by aerosol mass spectrometry, Johannes Gutenberg-Universität Mainz, Mainz, https://doi.org/http://doi.org/10.25358/openscience-3178, 2011.

Saha, Suranjana, Moorthi, Shrinivas, Wu, Xingren, Wang, Jiande, Nadiga, Sudhir, Tripp, Patrick, Behringer, David, Hou, Yu-Tai, Chuang, Hui-ya, Iredell, Mark, Ek, Michael, Meng, Jesse, Yang, Rongqian, Mendez, Malaqu?as Pe?a, van den Dool, Huug, Zhang, Qin, Wang, Wanqiu, Chen, Mingyue, and Becker, Emily: The NCEP Climate Forecast System Version 2, J. Clim., 27, 2185–2208,

https://doi.org/10.1175/JCLI-D-12-00823.1, 2014.

Salcedo, D., Onasch, T. B., Dzepina, K., Canagaratna, M. R., Zhang, Q., Huffmann, J. A., DeCarlo, P. F., Jayne, J. T., Mortimer, P., Worsnop, D. R., Kolb, C. E., Johnson, K. S., Zuberi, B., Marr, L. C., Volkamer, R., Molina, L. T., Molina, M. J., Cardenas, B., Bernabé, R. M., Márquez, C., Gaffney, J. S., Marley, N. A., Laskin, A., Shutthanandan, V., Xie, Y., Brune, W., Lesher, R., Shirley, T., and Jimenez, Jose L.: Characterization of ambient aerosols in Mexico City during the MCMA-2003 campaign with Aerosol Mass Spectrometry: Results from the CENICA Supersite, Atmos. Chem. Phys., 6, https://doi.org/10.5194/acp-6-925-2006, 2006.

Seinfeld, John H. and Pandis, S.N.: Atmospheric chemistry and physics: from air pollution to climate change., Third., John Wiley & Sons, Ltd, Hoboken, New Jersey, 2016.

Stein, A.F., Draxler, R.R., Rolph, G.D., Stunder, B.J.B., Cohen, M.D., Ngan, F., 2015. NOAA's HYSPLIT atmospheric transport and dispersion modeling system, Bull. Am. Meteorol. Soc. 96, 2059-2077, 10.1175/BAMS-D-14-00110.1.

Stohl, A, Hittenberger, M, and Wotawa, G: Validation of the Lagrangian particle dispersion model FLEXPART against large scale tracer experiment data, Atmos. Environ., 32, 4245–4264, 1998.

Tegen, Ina, Lacis, Andrew A., and Fung, Inez: The influence on climate forcing of mineral aerosols from disturbed soils, Nature, 380, https://doi.org/10.1038/380419a0, 1996.

von der Weiden, S.-L., Drewnick, F, and Borrmann, S: Particle Loss Calculator – a new software tool for the assessment of the performance of aerosol inlet systems, Atmos. Meas. Tech., 2, 479–494, https://doi.org/10.5194/amt-2-479-2009, 2009.